Journal of Solid State Chemistry **163,** 65–76 (2002)
doi:10.1006/jssc.2001.9370, available online at http://www.idealibrary.com on IDEAL®

Excess Oxygen in $LaMnO_{3+\delta}$

Keikichi Nakamura[1] and Keiichi Ogawa

Graduate School of Integrated Science, Yokohama City University, 22-2 Seto, Kanazawa-ku, Yokohama 2360027, Japan

Received May 29, 2001; in revised form August 16, 2001; accepted August 22, 2001

Using a volumetric method, the relationship among the oxygen desorption and absorption equilibrium pressure *P*, excess oxygen δ, and temperature *T* (*P*–δ–*T*) has been investigated for polycrystalline $LaMnO_{3+\delta}$. To interpret the measured *P*–δ–*T* relation, we have proposed a defect model in which La and Mn site vacancies exclude the formation of vacancies at their first and second nearest neighbors. The proposed model has been compared with other defect models derived on the basis of the law of mass action. The calculated *P*–δ–*T* relation has been favorably compared with the observed *P*–δ desorption isotherms. Significant deviations from the calculated relation, however, have been observed when the *P*–δ isotherm is acquired during the absorption process. This hysteretic behavior is attributed to the formation and annihilation of La and Mn site vacancies accompanied by the redox reaction. Using the present volumetric method, we are able to control the excess oxygen δ accurately by quenching the sample heat treated under appropriate oxygen equilibrium pressure. The X-ray diffraction and SQUID magnetization measurements on these oxygen-controlled samples are in good agreement with previous results. © 2002 Elsevier Science

Key Words: **defect chemistry; lanthanum manganite; oxygen nonstoichiometry; $LaMnO_3$; perovskite.**

1. INTRODUCTION

Excess oxygen problems in the lanthanum manganese oxide with or without the La and Mn site substitution have been extensively studied (1–12). The oxide prepared in air or in an oxygen atmosphere contains excess oxygen δ and is denoted by $La_{1-x}M_xMnO_{3+\delta}$ (*M*: Sr^{2+}, Ca^{2+}, vacancy, etc.). The amount of δ, however, is experimentally known to decrease with increasing doping level x at the La site to keep the Mn^{4+} proportion at nearly constant values, i.e., 26–36% (4, 7, 9, 11, 12). To understand thermodynamic properties of the excess oxygen and to control it over a wide range of temperatures and oxygen partial pressure, previous researchers have proposed various defect models (7, 9, 10). For example, the defect model proposed by Roosmalen and Cordfunke (7) has assumed the charge disproportionation reaction in which $2\xi Mn^{3+}$ are separated into ξMn^{2+} and ξMn^{4+} and only ξMn^{2+} could be oxidized to give ξMn^{3+}. The maximum Mn^{4+} proportion and oxygen deficiency, therefore, turned out to be ξ and $\xi/2$, respectively. This model fits fairy well with a certain range of experimental points and has been used to explain the dependence of δ on the Sr doping level x in thin films of $La_{1-x}Sr_xMnO_{3+\delta}$ ($x = 0.05$ to 0.14) (11).

Another model is a vacancy exclusion model proposed by Mizusaki *et al.* (9); La or Sr ions inside a sphere of influence defined at each cation vacancy are assumed not to participate in generating vacancies at all. Although both models fit well with a certain range of experimental points, they are based on the law of mass action and on the assumption that the activities of the species participating in the reaction are proportional to their concentration. Taking the above two models into consideration, we shall propose an improved defect model to explain the measured *P*–δ–*T* relation reasonably well.

2. EQUILIBRIUM EXCESS OXYGEN CONTENT AND REVISED DEFECT MODELS

2.1. A Defect Model Considering Entropy of Mixing

According to the defect chemistry of $LaMnO_{3+\delta}$ (7), the overall chemical reaction is described in the following way:

$$LaMnO_3 + \frac{\delta}{2}O_2 = \frac{3+\delta}{3}\{La^{3+}_{3/(3+\delta)}V_{\delta/(3+\delta)}\} \times \{Mn^{3+}_{3(1-2\delta)/(3+\delta)}Mn^{4+}_{3\cdot 2\delta/(3+\delta)}V_{\delta/(3+\delta)}\}O_3^{2-}. \quad [1]$$

Upon dissolution of $\frac{3}{2}$ oxygen molecules, therefore, 6 Mn^{4+} ions and 2 vacancies, i.e., 1 each at La and Mn site, are formed according to

$$6Mn^{3+} + \frac{3}{2}O_2 = 6Mn^{4+} + 3O^{2-} + V_{La} + V_{Mn}. \quad [2]$$

[1] To whom correspondence should be addressed. E-mail: keinaka@d9.dion.ne.jp.

0022-4596/02 $35.00

The equilibrium concentration of Mn^{4+}, V_{La}, V_{Mn}, and O^{2-} per formula unit of $3/(3+\delta)LaMnO_{3+\delta}$ are $3\cdot 2\delta/(3+\delta)$, $\delta/(3+\delta)$, $\delta/(3+\delta)$, and 3, respectively.

Equation [2] tells us that $\frac{3}{2}$ oxygen molecules in the gas phase and three oxygen ions in the solid $LaMnO_{3+\delta}$ phase are in equilibrium and therefore the chemical potentials of $\frac{3}{2}O_2$ and $3O^{2-}$ should be equal. To formulate the chemical potential per three oxygen ions, it is necessary to take account of the entropy of mixing for one vacancy at each La and Mn site and six Mn^{4+} ions. Here, we pay attention to the experimental fact that the amount of Mn^{4+} is independent of the Sr (or Ca) doping level x (4, 7, 9, 11, 12) for the samples annealed in air or oxygen and does not appear to exceed 36% (5). The maximum δ value in the literature lies around 0.36/2 to 0.35/2, i.e., 0.18 to 0.175, for $LaMnO_{3+\delta}$. According to Eq. [1], therefore, the maximum vacancy concentration in the La or Mn site is $\delta/(3+\delta) = 0.18/3.18 = 0.0566$. The maximum concentration 0.0566 implies that the first and second nearest neighboring sites (6 and 12 sites, respectively) around a La (Mn) site vacancy (18 sites total, resulting in the maximum vacancy concentration: $1/(18+1) = 0.0526$) are most likely to be unoccupied by another La (Mn) site vacancies. In the following we simply assume the maximum δ value, $\delta_{max} = 0.18$, since $LaMnO_{3.18}$ has been reported to form when annealed at 1073 K in 1 atm oxygen (5). Assuming the random mixing of Mn^{4+} ions and taking account of the Mn^{4+} concentration, the term $3\cdot 2\delta/(3+\delta)$ in Eq. [1] must be divided by the total Mn concentration $3/(3+\delta)$, and then we obtain the following expression for the chemical potential of three oxygen ions:

$$3\mu_O = 3\mu_O^\circ(T) + RT \ln \left\{\frac{\eta\delta/(3+\delta)}{1-\eta\delta/(3+\delta)}\right\}^2 + RT \ln \left(\frac{2\delta}{1-2\delta}\right)^6$$
$$= 3\mu_O^\circ(T) + RT \ln f_{ex}(\delta). \quad [3]$$

The first term in the right-hand side of Eq. [3], i.e., $3\mu_O^\circ(T)$, is the standard potential at temperature T, the second term arises from the entropy of mixing of La and Mn site vacancies, and the third term from the entropy of mixing of six Mn^{4+} ions. The parameter η is adjustable and can be determined experimentally from the maximum excess oxygen value $\delta_{max} = 0.18$ as $\eta^{-1} = \delta_{max}/(1+\delta_{max}) = 0.0566$. η turns out to be 17.67 in the present case. η is also related to the number of nearest neighboring sites around a La(Mn) vacancy excluding the formation of another vacancy. At the equilibrium, the chemical potentials of oxygen in the gas and solid phases must be equal:

$$\tfrac{3}{2}\mu_{O_2} = 3\mu_O. \quad [4]$$

Since $\mu_{O_2} = \mu_{O_2}^\circ(T) + RT \ln P_{O_2}$, then we obtain the following equation,

$$\tfrac{3}{2} RT \ln P_{O_2} = \Delta\mu^\circ(T) + RT \ln f_{ex}(\delta), \quad [5]$$

where $\Delta\mu^\circ(T) = 3\mu_O^\circ(T) - (\frac{3}{2})\mu_{O_2}^\circ(T)$ is the standard relative potential for the reaction. To be consistent with the definition K for the defect models based on the law of mass action, the equilibrium constant for the present exclusion model, K_{ex}, is defined as

$$K_{ex} = \exp\left\{\frac{(\frac{3}{2})\mu_{O_2}^\circ(T) - 3\mu_O^\circ(T)}{RT}\right\} = \exp\left\{\frac{-\Delta\mu^\circ(t)}{RT}\right\}. \quad [6]$$

Using eqs. [3] to [5], we obtain

$$K_{ex} = f_{ex}(\delta)\, P_{O_2}^{-3/2}. \quad [7]$$

In the above calculation, we ignored the interaction energy between Mn^{3+} and Mn^{4+} ions. Such interaction would be important only when the temperature range is close to the charge ordering transition temperature ($< 300 \cong 200$ K) and when the Mn^{4+} proportion is close to a particular Mn^{3+} to Mn^{4+} ratio (1:1 in most cases). It is noted that the ranges of the temperature and Mn^{4+} proportion of our interest are far from the charge ordering condition stated above.

2.2. *Comparison with the Other Defect Models*

Roosmalen and Cordfunk (7) have presented several defect models. One model takes account of the upper limit of δ by considering the charge disproportionation of Mn^{3+} into Mn^{2+} and Mn^{4+}. They have introduced a parameter, ξ, i.e., the amount of Mn^{2+} and M^{4+} formed by the disproportionation of Mn^{3+}. The upper limit of Mn^{4+} (δ) is, therefore, given by ξ ($\xi/2$) when ξ Mn^{2+} ions are completely converted to ξMn^{3+} upon the uptake of oxygen. This model explains the P–δ–T relation observed $\delta > 0.03$ and at relatively higher P_{O_2}, i.e., 10^3 to 10^5 Pa. This model is also successful in explaining quantitatively the relation among the Sr doping level x, excess oxygen δ, and pressure P_{O_2} (11). A drawback of this model is the very assumption of the charge disproportionation; this assumption is not satisfied for various similar compounds in which charge disproportionation is unlikely to occur. Here, we assume a similar vacancy exclusion concept to formulate a modified defect model on the basis of the law of mass action to demonstrate that the result is completely coincident with Eq. [3].

The equilibrium constant K for the reaction in Eq. [2] is given by

$$K = [Mn^{4+}]^6[O^{2-}]^3[V_{La}]\cdot[V_{Mn}][Mn^{3+}]^{-6}P_{O_2}^{-3/2}. \quad [8]$$

Since the simple proportional relation between the concentration and activity breaks down when δ approaches δ_{max}, the activities of La and Mn site vacancies can be better

expressed as $\{(\eta\delta/(3+\delta))/(1-\eta\delta/(3+\delta))$, where $\eta^{-1} = 1/17.67$ is the upper limit of vacancy concentration, i.e., 0.18/3.18 in this case. With substitution of $[Mn^{4+}] = 3\cdot 2\delta/(3+\delta)$, $[Mn^{3+}] = 3\cdot(1-2\delta)/(3+\delta)$ and $[O^{2-}] = 3$ into Eq. [8], we obtain the following equation,

$$K = \frac{(2\delta)^6 3^3 \{\eta\delta/(3+\delta)\}^2}{(1-2\delta)^6\{1-\eta\delta/(3+\delta)\}^2} P_{O_2}^{-3/2} \equiv f(\delta)\, P_{O_2}^{-3/2}. \quad [9]$$

The temperature dependence of K is given by

$$\ln K = \frac{-\Delta H_v^\circ/R}{T} + \frac{\Delta S_v^\circ}{R}. \quad [10]$$

Comparison of Eqs. [3] and [9] shows that both functions $f_{ex}(\delta)$ and $f(\delta)$ are of the same form except for that an additional constant 3^3 (fixed oxygen concentration) is noted in Eq. [9].

We use Roosmalen's value 45,700 for $-\Delta H_v^\circ/R$ in our calculation below. Since the $f(\delta)$ function in Eq. [9] differs from the $f(\delta)$ function given in Ref. (7) (see Eq. [13]), we set $\Delta S_v^\circ/R = -39.6$ by assuming that Eqs. [9] and [13] give the same P_{O_2} at $\delta = 0.1$. The temperature dependence of K is thus given by

$$\ln K = \frac{45{,}700}{T} - 39.6. \quad [11]$$

Similarly, we obtain $\ln K_{ex}$ for the present defect exclusion model by considering the difference in $\ln f_{ex}(\delta)$ and $\ln f(\delta)$, i.e., $3 \ln 3 = 3.296$ and K_{ex} is given by

$$\ln K_{ex} = \frac{45{,}700}{T} - 42.9. \quad [12]$$

The difference between Eqs. [3], [7], and [9] arises from the way we count the contribution of Mn^{4+} ions. The present exclusion model, i.e., Eqs. [3] and [7], is based on the random mixing of Mn^{4+} and Mn^{3+} ions, whereas the modified defect model is based on the law of mass action and on the assumption that the activities of Mn^{3+} and Mn^{4+} ions are proportional to the corresponding concentrations. Since Eqs. [3] and [9] turn out to be the same except for the constant term 3^3 and since the constant term could be included in K, $f_{ex}(\delta)$ instead of $f(\delta)$ will be used hereafter.

Figure 1 compares P–δ isotherms at $T = 1073$ and 1573 K evaluated for three different models, i.e., the vacancy exclusion model (Eqs. [3] and [7]), Roosmalen's defect model (hereafter denoted as R model), and Mizusaki's vacancy exclusion sphere model taking only the La side vacancies into account (hereafter denoted as M model).

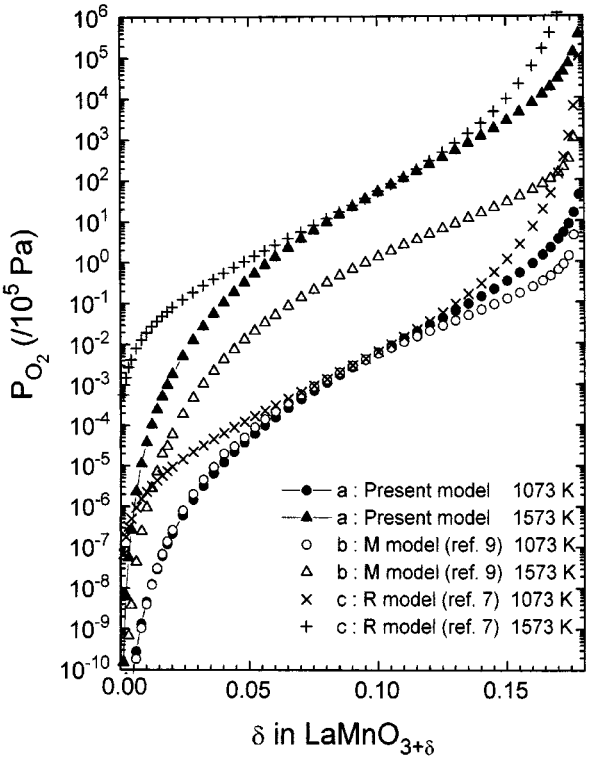

FIG. 1. Comparison of P–δ–T isotherms of $LaMnO_{3+\delta}$ calculated on the basis of three different models. a, present model (Eqs. [3], [7] and [12]). b, Mizusaki *et al.* (Ref. (9), Eqs. [15] and [16]). c, Roosmalen and Cordfunke (Ref. (7), Eqs. [13] and [14]).

Equations derived on the basis of the R models are

$$K_R = \frac{(1-2\xi+2\delta)^6 3^3 \delta^2}{(\xi-2\delta)^6(3+\delta)^2} P_{O_2}^{-3/2}, \quad [13]$$

where $\xi = 0.352$ for $LaMnO_{3+\delta}$, and

$$\ln K_R = \frac{45{,}700}{T} - 32. \quad [14]$$

For the M model, P_{O_2} is given by

$$K_M = 2^{-1}\cdot 3^6 \left(\frac{2\delta}{3+\delta}\right)^9 \left(\frac{3+\delta}{3-17\delta}\right) P_{O_2}^{-3/2} \quad [15]$$

and

$$\ln K_M = \frac{27{,}630}{T} - 25.9. \quad [16]$$

The factor $(3-17\delta)$ appearing in Eq. [15] becomes zero at the upper limit of δ_{max}, i.e., $\delta = 3/17 = 0.176$. The P–δ–T

isotherms calculated at 1073 K are in good agreement between the present vacancy exclusion model and the M model, particularly in the low δ region less than 0.1. A significant difference between the two isotherms evaluated at 1573 K is noted and is attributed to the difference in the enthalpy of vacancy formation, $-\Delta H_v^\circ/R$, i.e., 45,700 and 27,630. We prefer 45,700 to 27,630 for $-\Delta H_v^\circ/R$ because the previous study on the excess oxygen in $La_{1-x}Sr_xMnO_{3+\delta}$ (11) demonstrates that the temperature dependence of the P–δ–T relation can be better described when $-\Delta H_v^\circ/R =$ 45,700.

The two isotherms (1078 and 1578 K) for the present model shown in Fig. 1 deviate significantly in the low δ region from those for the R model. The deviation arises from the different formulation concerning the upper limit of δ, namely, $\{\eta\delta/(3+\delta)\}/\{1-\eta\delta/(3+\delta)\}$ in Eq. [3] and $(1-2\xi+2\delta)/(\xi-2\delta)$ in Eq. [13]. The function of configurational entropy for the La and Mn site vacancies, i.e., $\ln f_c(\delta) = \ln[\eta\delta/(3+\delta)/\{1-\eta\delta/(3+\delta)\}]$ given in Eq. [3] shows $\frac{1}{2}$ rotational symmetry with respect to the midpoint, i.e., $\eta\delta/(3+\delta) = 0.5$. The corresponding term expressing the upper limit of δ for the R model, $(1-2\xi+2\delta)/(\xi-2\delta)$, is given by the ratio of Mn^{3+} to Mn^{2+} and is determined from the degree of disproportionation ξ and oxidation (defect formation) δ and has no such $\frac{1}{2}$ rotational symmetry as the $f_c(\delta)$ function shows.

3. EXPERIMENTAL

Polycrystalline $LaMnO_{3+\delta}$ samples were prepared by a conventional solid-state reaction method. The reagents, La_2O_3 and Mn_3O_4, as received were fired at 1573 K in air and at 1073 K in the flowing oxygen, respectively. It was found that the commercially available La_2O_3 contained about 3.7 to 4.2% of eliminated components such as H_2O and CO_2. The purity of Mn_2O_3, converted from the heat-treated Mn_3O_4 reagent, was checked by measuring the SQUID magnetization. No ferromagnetic component Mn_3O_4, ($T_c = 45$ K) was detected at all after the heat treatment, whereas the as-received Mn_3O_4 was found to contain as much as 25% Mn_2O_3 (estimated from the 2.62% increase in weight).

$LaMnO_{3+\delta}$ and $La_{0.97}MnO_{3+\delta}$ polycrystalline samples were synthesized by the conventional solid-state reaction method. The well-mixed powder of La_2O_3 and Mn_3O_4 was first calcined at 1473 K for 20 h, then grounded, and finally heated at 1573 K for 20 h. The precursor powder thus-prepared was then formed into a pellet of low density with adding low pressure and again heated to 1573 K for 15 h. The pelletized samples were further heated in the flowing oxygen at 1223 K for 20 h and then furnace cooled. The pelletized samples thus-fabricated were found porous (easily broken, 0.5–0.7 times the theoretical density) and resulted in the fast absorption and desorption reaction.

The excess oxygen contents in some $LaMnO_{3+\delta}$ compounds were determined by measuring the amount of oxygen gas desorbed or absorbed from the $LaMnO_{3+\delta}$ samples using the pressure–composition–temperature (PCT) relation measuring system (13), equipped with two capacitant manometers (10 and 100 Torr full range) as schematically shown in Fig. 2. The measuring procedure is as follows: a small fragment of pelletized sample (about 0.3–0.5 g) was placed in a quartz reaction vessel and was evacuated to eliminate absorbed gases and to obtain the lower background pressure. Prior to the desorption experiment, V_1 and V_2 were opened and V_3 and V_4 were closed. The quartz reaction tube was then heated at a heating rate of 20 K/min. During the heating and evacuating process below 873 K, three desorption peaks were found and denoted as P_1, P_2, and P_3 (Fig. 3). The peak heights vary depending on the vacuum pre-treatment of the measuring system (compare desorption curve a with b). Repeated high-temperature (1173 K) vacuum pre-treatments of the quartz reaction tube reduced these desorption peak heights and the background pressure. The first peak, P_1, appearing around 473 K is ascribed to the desorption of H_2O absorbed on the surface

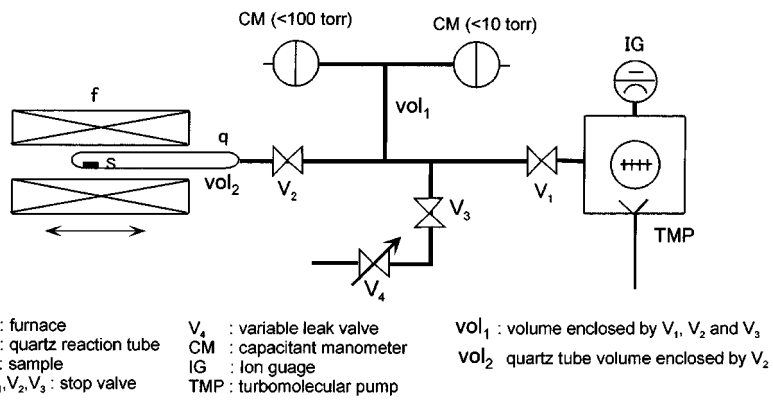

FIG. 2. Schematic diagram of the present volumetric apparatus.

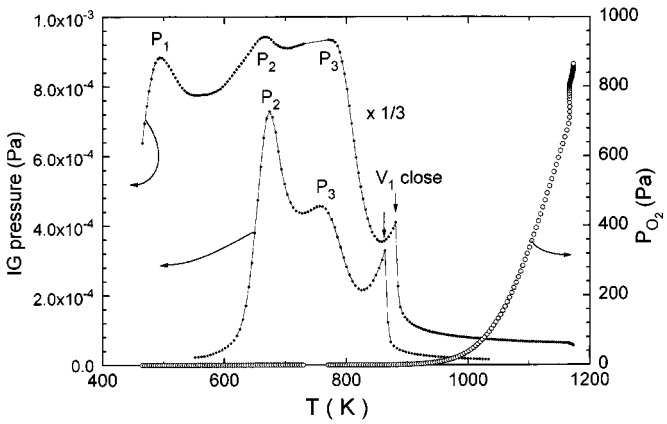

FIG. 3. Temperature-programmed desorption spectra of $LaMnO_{3+\delta}$ sample under dynamic evacuation and the oxygen partial pressure increase in the system after closing valve V_1. The temperature increasing rate is 30 K/min unto 1173 K and the temperature is kept constant at 1173 K. The different desorption curves a and b are due to the different vacuum and heat pretreatments of the system.

of a quartz glass tube and the second and third peaks, P_2 and P_3, can be ascribed to the desorption of H_2O from the inside of quartz tube (14). The fourth strongest desorption peak (only the initial tail part of which is seen in Fig. 3) began to appear above 873 K and can be ascribed to the oxygen degassing from the manganite sample. In this experiment, the valve V_1 was then closed at this temperature and the oxygen partial pressure in the system was allowed to increase with the temperature, which increased at a rate of 30 K/min. The nearly vertical increase in P_{O_2} observed at $T = 1173$ K implies that the oxygen desorption rate was not fast enough to follow the rate of temperature increase and that the pressure increase due to the oxygen desorption continued until the equilibrium pressure was attained at the plateau temperature of 1173 K.

The X-ray diffraction (XRD) measurements were performed with a RINT system (RIGAKU) using Cu$K\alpha$ radiation. Magnetization measurements were made with a Quantum Design MPMS system in a field of 500 Oe with zero field cooling (ZFC) and field cooling (FC) modes.

4. RESULTS

Figure 4 shows the oxygen desorption vs time curves for a continuous desorption process, measured using the system shown in Fig. 2. The valve operation at each step is marked by C_1 (V_1 close), C_2 (V_2 close $\rightarrow$ V_1 open) and C_3 (V_1 close $\rightarrow$ V_2 open). The first step of the desorption curve taken during the increasing temperature from 873 to 1173 K is the same one as shown in Fig. 3. After attaining the equilibrium at 1173 K, the reaction system underwent the operation C_2 and the oxygen gas enclosed by V_1, V_2, and V_3 (volume vol_1) was evacuated and then the system underwent the operation C_3 to initiate the second desorption step. The amount of oxygen gas desorbed from the sample can be evaluated from the equilibrium pressure and volume of the system ($vol_1 + vol_2$). Taking into account the background pressure due to the residual pressure (P_{1e}) in the reaction tube (vol_2), we calculate the net pressure increase ΔP in the system due to the desorption of oxygen in the second step as follows:

$$\Delta P = P_{2e} - P_{1e}\frac{vol_2}{vol_1 + vol_2}, \qquad [17]$$

where P_{1e} and P_{2e} are the equilibrium pressures immediately before the operation C_2 for the first and second desorption processes, respectively. Since there is a time lag between the closing of V_2 and opening of V_1 in the operation C_2 and since vol_1 and vol_2 decrease due to the closing operation of V_2, P_e increased a little bit (0.2%), as seen in Fig. 4. Similar valve operations, C_2 and C_3, were repeated four times in Fig. 4. After completing the fifth desorption process, we carried out several different operations. One is to quench the sample to room temperature to see the weight and lattice constant changes. Another is to perform an absorption process immediately after completing the final desorption process or to continue the desorption process further in vacuum or at constant partial pressure (10^{-4} to 10^{-5} Pa) under dynamic vacuum attained by opening the valves V_1 and V_2.

Figure 5 shows a series of absorption processes of the sample, which was evacuated for 30 min following the desorption processes shown in Fig. 4. A sequence of valve operations is shown in Fig. 5. The oxygen gas here was

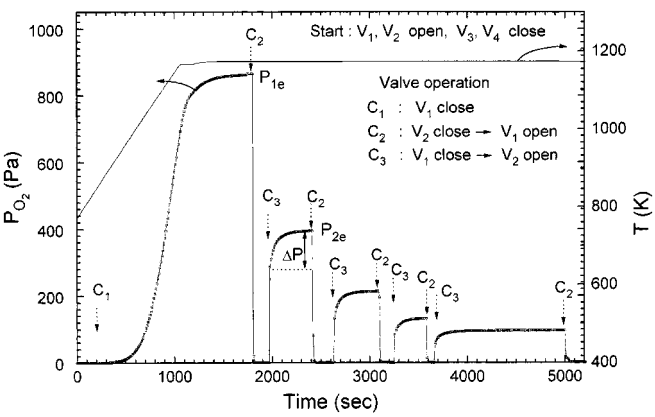

FIG. 4. Oxygen desorption curves for $LaMnO_{3+\delta}$ measured during a series of continuous desorption processes under increasing (873 to 1173 K) and constant temperature (1173 K). The programmed temperature of the system is shown in the figure. Sequence of the valve operation C_1 to C_3 is marked with arrows.

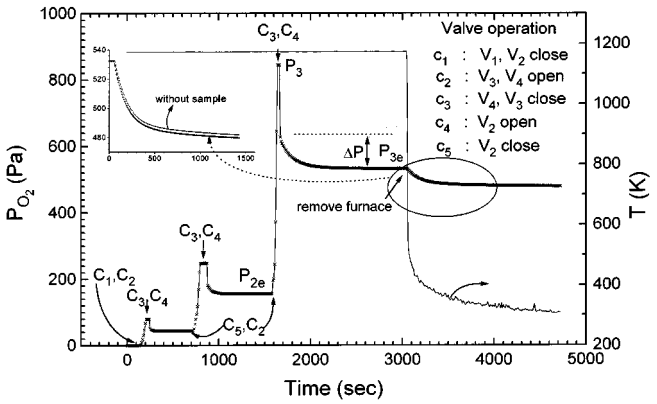

FIG. 5. Oxygen absorption curves for $LaMnO_{3+\delta}$ measured during a series of continuous absorption processes at a constant temperature of 1173 K. Sequence of the valve operation C_1 to C_5 are marked with arrows. The inset to the figure shows pressure change during the rapid cooling with and without $LaMnO_{3+\delta}$ sample.

introduced into the system using the variable leak valve V_4. As in the desorption process, the initial pressure decrease just after the operation C_4 must be taken into account to estimate the net pressure decrease ΔP due to the absorption of oxygen. For the third absorption process, for example, ΔP is given by

$$\Delta P = \frac{P_{2e}\,\mathrm{vol}_2 + P_3\,\mathrm{vol}_1}{\mathrm{vol}_1 + \mathrm{vol}_2} - P_{3e}, \qquad [18]$$

where P_3 is the pressure just before the operation C_4 and P_{2e} and P_{3e} are the equilibrium pressures in the second and third absorption processes, respectively (Fig. 5). After the final absorption step (i.e., the third in Fig. 5), the quartz reaction vessel was allowed to cool rapidly to room temperature by removing the furnace. The pressure decrease in the cooling step was mostly due to the decrease in the oxygen gas temperature. The amount of oxygen gas absorbed in the rapid cooling process was obtained by referring to the pressure decrease without sample as shown in the inset to Fig. 5. The net decrease due to the oxygen absorption during this rapid cooling was ca. 10^{-5} in δ value and could be neglected.

The amount of oxygen gas desorbed or absorbed can be accurately determined by the volumetric method mentioned above. However, the initial excess oxygen value δ (denoted as δ_0) in the as-prepared sample cannot be determined by the volumetric method. Most research groups have determined the excess oxygen δ from the Mn^{4+} concentration by assuming that the cationic ratio Mn/La or Mn/(La + M) is accurately determined. It should be noted, however, that the generation of 1% La or Mn site vacancies results in a 3% increase of Mn^{4+}, which in turn causes 1.5% overestimation of the excess oxygen value. In the present work, we have estimated the Mn^{4+} concentration by comparing the measured lattice parameters with those from the published data, but the accuracy of this method depends on that of the experimentally determined La/Mn ratio. We have also measured the weight change after the oxygen reduction in dynamic vacuum at 1173 K but the weight loss due to this reduction treatment is about 0.6% for the change $\Delta\delta = 0.1$, i.e., about 3.0 mg for a sample of 0.5 g. The accuracy of this method is in excess of $\pm$ 10%, owing to our balance accuracy.

Figure 6 shows X-ray diffraction (XRD) patterns of some $LaMnO_{3+\delta}$ samples of which the excess oxygen value δ was varied by the oxygen treatment at different absorption and desorption pressures (see the caption of Fig. 6). These patterns show a clear rhombohedral (a) to orthorhombic (d, e, and f) phase change as the excess oxygen value δ varies. However, a close examination of the patterns b and c shows superposed patterns coming from both phases, implying the coexistence of the two phases. Table 1 lists the desorption or absorption pressures, lattice parameters, and cell volumes. Judging from the relations of the lattice parameter δ (5–7) and of P–δ–T in Fig. 1, the lattice parameters must be smaller for the sample treated in higher oxygen partial pressure. However, the perovskite lattice parameter $a_p = 3.965$ A ($a = 5.523$, $b = 5.662$, $c = 7.707$) for the sample treated at the absorption pressure of 537 Pa ($\delta = 0.049$) is larger than $a_p = 3.935$ A ($a = 5.519$, $b = 5.592$, $c = 7.725$) for the sample treated at the desorption pressure of 118 Pa ($\delta = 0.073$). Later, we will show that this unusual phenomenon is due to the hysteretic behavior of the P–δ–T relation.

The lattice parameters are plotted in Fig. 7 as a function of the unit cell volume V_c per four formula units in Fig. 7. The diffraction lines at the boundary between the

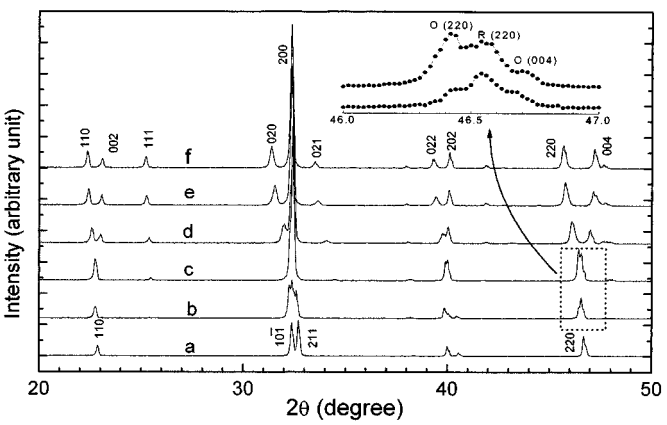

FIG. 6. X-ray diffraction patterns for $LaMnO_{3+\delta}$ rapidly cooled from 1173 (c–f) and from 1073 K (b) under various absorption (abs) and desorption (des) equilibrium oxygen pressure. a, as-prepared (1223 K, 10^5 Pa); b, 208 Pa, des; c, 9320 Pa, abs; d, 118 Pa, des; e, 527 Pa, ab; f, 0.8 Pa, des.

TABLE 1
Lattice Parameters of $LaMnO_{3+\delta}$ and $La_{0.97}MnO_{3+\delta}$ Rapidly Cooled from 1173 K (*b*: 1073 K) under Various Desorption and Absorption Equilibrium Pressures

P_{O_2} (/10^5 Pa)		Lattice parameters	δ	XRD[a]	M–T[b]
		$LaMnO_{3+\delta}$			
0.00527	Absorption	$a = 5.523$, $b = 5.662$, $c = 7.707$, $a_p = 3.965$, $V_c = 241.0$[c]	0.049	e	
0.000008	Desorption	$a = 5.526$, $b = 5.694$, $c = 7.701$, $a_p = 3.974$, $V_c = 242.28$	0.033	f	
0.00009	Desorption	$a = 5.525$, $b = 5.652$, $c = 7.722$, $a_p = 3.958$, $V_c = 241.13$	0.049	g	
0.00118	Desorption	$a = 5.519$, $b = 5.592$, $c = 7.725$, $a_p = 3.935$, $V_c = 238.42$	0.073	d	b
0.01390	Absorption	$a = 5.5234$, $b = 5.543$, $c = 7.793$, $a_p = 3.916$, $V_c = 238.59$	0.072	h	
0.09323	Absorption[d]	$a = 5.519$, $b = 5.542$, $c = 7.770$, $a_p = 3.909$, $V_c = 237.64$	0.086	c	
Vacuum (60 min)	Desorption	$a = 5.527$, $b = 5.694$, $c = 7.705$, $a_p = 3.974$, $V_c = 242.46$	0.030		c
0.00208 (1073 K)	Desorption[d]	$a = 5.4790$, $\alpha = 60.75°$, $a_p = 3.892$, $V_c = 236.5$	0.105	b	
As-prepared (1223 K × 20 h in O_2)		$a = 5.474$, $\alpha = 60.59°$, $a_p = 3.887$, $V_c = 235.1$	0.145	a	a
			Mn^{4+} (%)		
		$LaMn_{0.97}MnO_{3+\delta}$			
0.00005	Desorption	$a = 5.5305$, $b = 5.673$, $c = 7.725$, $a_p = 3.963$, $V_c = 242.37$	7.8		
0.007533	Absorption	$a = 5.524$, $b = 5.670$, $c = 7.715$, $a_p = 3.963$, $V_c = 241.64$	8.2		
0.00185	Desorption	$a = 5.523$, $b = 5.611$, $c = 7.741$, $a_p = 3.945$, $V_c = 239.86$	11.8		b
0.00526	Desorption	$a = 5.521$, $b = 5.586$, $c = 7.766$, $a_p = 3.934$, $V_c = 239.17$	12.8		
Vacuum (80 min)	Desorption	$a = 5.533$, $b = 5.714$, $c = 7.710$, $a_p = 3.975$, $V_c = 243.72$	4.0		c
As-prepared (1223 K × 20 h in O_2)		$a = 5.470$, $\alpha = 60.70°$, $a_p = 3.888$, $V_c = 235.1$	29		a

[a] Corresponding XRD patterns, a–e, are shown in Fig. 6a–g referred in Fig. 10.
[b] Corresponding M–T curves, a–c are shown in Figs. 11a and 11b.
[c] Volume in 10^{-24} cm^3 (per four formula units).
[d] Two-phase mixed reflections shown by b and c in Fig. 6.

orthorhombic ($V_c > 237.8$) and rhombohedral ($V_c < 236.5$) phases show the coexistence of both phases as shown by the patterns b and c in Fig. 6 and the lattice parameters showing the mixed patterns of the two phases are marked by closed symbols. The observation of the two-phase coexistent region is in agreement with the studies on $LaMnO_{3+\delta}$ (5) and $La_{1-x}Sr_xMnO_{3+\delta}$ (15). In the two-phase region, only the relative diffraction intensities of the orthorhombic and rhombohedral phases change and the lattice parameters and unit cell volume of the two phases are kept fixed at their terminal values.

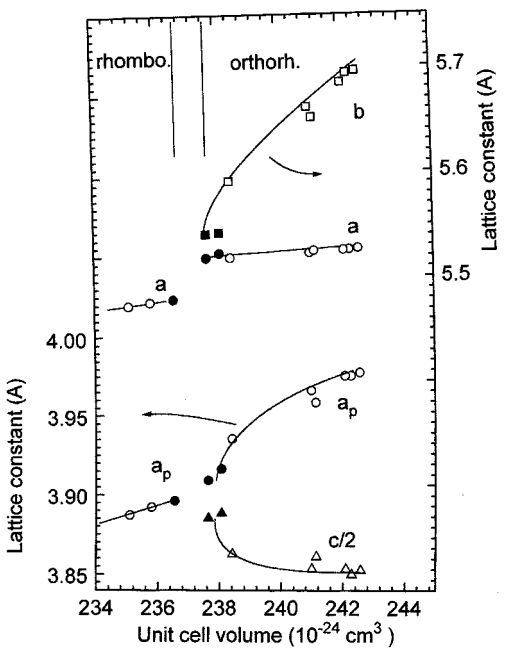

FIG. 7. Lattice parameters of $LaMnO_{3+\delta}$ as a function of unit cell volume. Closed marks at the orthorhombic and rhombohedral phase boundaries are derived from the superposed diffraction patterns of the two phases.

It is known that the perovskite unit cell parameter a_p in the rhombohedral region of $La_{1-x}Sr_xMnO_{3+\delta}$ is a linear function of the Mn^{4+} concentration (11, 16). In epitaxial thin films where only a_p can be estimated from the conventional θ–2θ scan, the excess oxygen value δ was estimated from a_p (11). To evaluate the δ value in polycrystalline samples, the unit cell volume is considered to be preferable to the lattice parameters. Roosmalen *et al.* (17) have shown that a number of experimental data can be fitted with a third-order polynomial, i.e.,

$$V_c = (244.55 - 24.97 \cdot \delta - 850.0 \cdot \delta^2 + 3918 \cdot \delta^3)10^{-24}\ \text{cm}^3. \quad [19]$$

This polynomial is plotted in Fig. 8 as a function of δ and is shown by a thick line.

First, we tentatively determine δ with the aid of the P–δ isotherm at 1173 K calculated from Eqs. [3], [7], and [12]

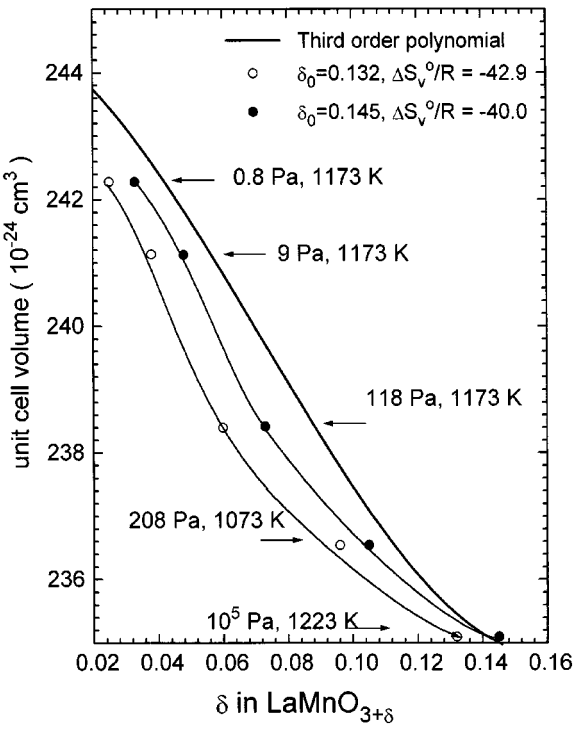

FIG. 8. Unit cell volumes as a function of δ for $LaMnO_{3+\delta}$. The thick line is drawn according to Eq. [19]. Open and closed circles are calculated from the theoretical P–δ isotherms at 1173 K assuming $\Delta S_v^\circ/R$ to be -42.9 and -40.0, respectively.

(see the closed marks (1073 and 1573 K) in Fig. 1, for example). To do this, the observed dissociation pressures for the rapidly cooled samples (see d and f in Fig. 6 and g in Table 1) are plotted on the P–δ isotherm at 1173 K to determine the relation between the tentative δ and the unit cell volume. The tentative δ values and corresponding dissociation pressures are given by 0.06 (118 Pa), 0.048 (9 Pa), and 0.025 (0.8 Pa). The δ_0 value for the as-prepared $LaMnO_{3+\delta}$ is then determined from the $\Delta\delta$ value of 0.073 for the desorption pressure of 118 Pa and the tentative δ value of 0.060 given above using the relation $\delta_0 = \delta + \Delta\delta = 0.132$. Some sets of δ's and unit cell volumes thus obtained are plotted by open circles in Fig. 8. The plotted V_c–δ curve deviates significantly from the polynomial curve, suggesting that the P–δ curve in Fig. 1 should be shifted somewhat to the lower pressure side when the P–δ relation is measured during the desorption process. The second trial is to evaluate the δ_0 value for the as-prepared $LaMnO_{3+\delta}$ from the unit cell volume, $V_c = 235$ and Eq. [19]. The resultant δ_0 is 0.145. Then, using the amount of desorbed oxygen, $\Delta\delta$ and the desorption pressure relation shown in Fig. 4, we obtain the P–δ ($\delta = \delta_0 - \Delta\delta$) relation as shown in the first block of Table 2. Improved P–δ isotherms based on Eqs. [3]–[7] are then determined to fit the observed points by adjusting the $\Delta S_v^\circ/R$ value from -42.9 (Eq. [12]) to -40.0 while keeping $-\Delta H_v^\circ/R = 45{,}700$ constant. We define the following constant K_d as the equilibrium constant for the oxygen dissociation of $LaMnO_{3+\delta}$:

$$\ln K_d = \frac{45{,}700}{T} - 40.0. \qquad [20]$$

This equilibrium constant K_d is by the factor exp (-0.6667×2.9) lower than the equilibrium pressure given in Fig. 1. Based on this P–δ–T relation, we obtain V_c vs δ relation in the desorption process and some of them are listed in Table 1. The δ–V_c curve thus obtained is located closer to the polynomial curve (see closed circles in Fig. 8). Table 2 summarizes the relative and absolute excess oxygen values thus estimated from the volumetric and unit cell volume measurements. In the absorption process shown in Table 2, $\Delta\delta$ means oxygen increase from the deoxidized state; namely, $\delta = \delta_{deox} + \Delta\delta$ and the δ_{deox} values were

TABLE 2
***P*–δ–*T* Isotherm Data for $LaMnO_{3+\delta}$ at 1173 K**

Desorption ($\delta_0 = 0.145$)			Absorption ($\delta_{deox} = 0.027$)			Absorption ($\delta_{deox} = 0.0406$)		
P_{O_2} (/10^5 Pa)	$\Delta\delta$	$\delta = \delta_0 - \Delta\delta$	P_{O_2} (/10^5 Pa)	$\Delta\delta$	$\delta = \delta_{deox} + \Delta\delta$	P_{O_2} (/10^5 Pa)	$\Delta\delta$	$\delta = \delta_{deox} + \Delta\delta$
0.00852	0.0533	0.0917	0.0010	0.0070	0.034	0.000436	0.00055	0.0412
0.0039	0.0608	0.0842	0.0046	0.0158	0.0428	0.00153	0.00239	0.0430
0.00212	0.0665	0.0785	0.0098	0.0298	0.0568	**0.00527**	**0.00840**	**0.0490**
0.00131	0.0704	0.0746	0.0134	0.0352	0.0622	$\delta_{deox} = 0.0490 - 0.0084$		
0.00095	0.0730	0.0720	0.0216	0.0414	0.0684	Absorption ($\delta_{deox} = 0.067$)		
1.000	0.0	0.145	0.04348	0.0497	0.0765	0.00505	0.0014	0.0684
0.00118	**0.0720**	**0.0730**	**0.09323**	**0.0590**	**0.0860**	0.01034	0.0037	0.0707
$\delta_0 = 0.072 + 0.073$			$\delta_{deox} = 0.0860 - 0.0590$			**0.01390**	**0.0050**	**0.0720**
						$\delta_{deox} = 0.0720 - 0.0050$		

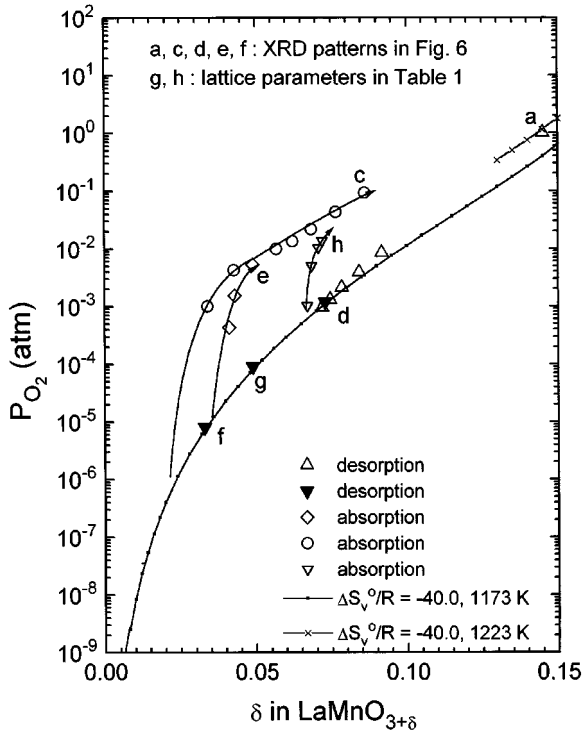

FIG. 9. P–δ–T isotherms measured during the desorption and absorption processes (Figs. 4 and 5). Symbols a, c, d, e, and f in the figure correspond to XRD patterns of a, c, d, e, and f in Fig. 6. Lattice parameter data for symbols g and h are listed in Table 1.

determined from the δ values of the rapidly cooled samples (Table 2 with bold letters).

In Fig. 9 the excess oxygen values summarized in Table 2 are plotted on the P–δ–T desorption isotherms of $LaMnO_{3+\delta}$, which is calculated from the dissociation equilibrium constant K_d given by Eq. [20]. We note that the hysteretic effects are observed when the P–δ measurement is carried out for the desorption and then for the absorption processes successively. The hysteresis was enhanced substantially when the sample was deoxidized in oxygen gas of a lower partial pressure. The absorption equilibrium pressure is always higher than the desorption equilibrium pressure. In other words, excess oxygen partial pressure is necessary to incorporate oxygen than to remove oxygen. In Fig. 10, the observed dissociation pressures are plotted as a function of δ on the desorption isotherms assuming the dissociation equilibrium constant K_d given by Eq. [20]. All the experimental points between 1073 to 1273 K show good agreement with the calculated isotherms.

Figures 11a and 11b show the temperature dependence of magnetization measured in a field of 500 Oe (FC and ZFC) for $LaMnO_{3+\delta}$ and $LaMn_{0.97}O_{3+\delta}$ with different oxygen reduction. Together with the XRD patterns shown in Fig. 6, these data provide us a measure showing how accurately the present volumetric method has controlled the excess oxygen potential. Referring to the T_c vs δ relation by Toepfer and Goodenough (5, 6), the Curie temperature T_c of the present as-prepared $LaMnO_{3+\delta}$ sample, i.e., 200 K, corresponds to $\delta = 0.15$, which is almost equal to 0.145, estimated from the unit cell volume.

It is also noted in Figs. 11a and 11b that a slight decrease in the Mn proportion from the stoichiometric value decreases T_c by about 60 K for the as-prepared samples, (ZFC curves a's in Figs. 11a and 11b resulting in $T_c = 200$ and 140 K, respectively). The lowest T_c of ca. 110 K is found for the $LaMn_{0.97}O_{3+\delta}$ sample rapidly cooled from 185 Pa oxygen partial pressure (b in Fig. 11b, 10% Mn^{4+} from Table 1), which is about 60 K lower than the corresponding $LaMnO_{3+\delta}$ with the same Mn^{4+} proportion (170 K from Ref. (6)). This observation suggests that the Mn/La ratio of the present samples is accurately controlled and a slight change in the La/Mn ratio around the stoichiometric ratio affects the physical properties strongly.

5. DISCUSSION

5.1. Cation Vacancy Sites and P–δ–T Relation

It is generally accepted that nonstoichiometry of excess oxygen in $LaMnO_{3+\delta}$ is accompanied by cation vacancies, either at the La and Mn sites in equal amounts (5, 7) or

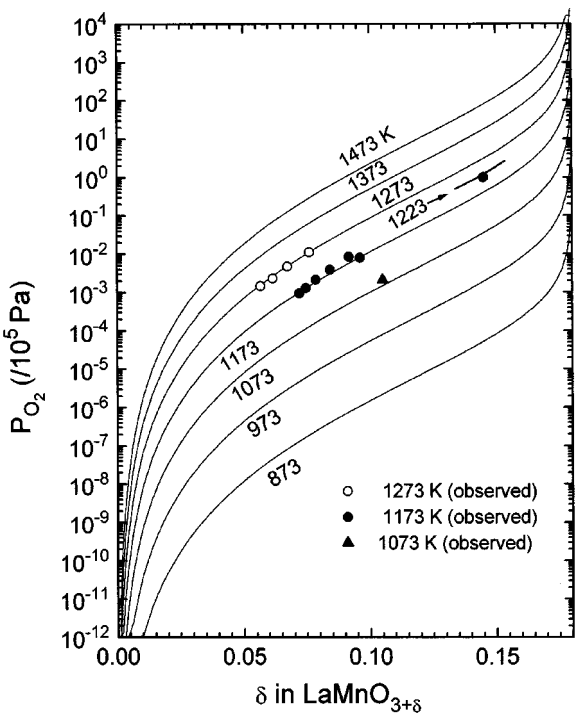

FIG. 10. The experimental P–δ data are plotted on the desorption P–δ–T isotherms at temperatures from 873 to 1463 K for $LaMnO_{3+\delta}$, which are calculated on the basis of the present model (Eqs. [3], [7] and [20]).

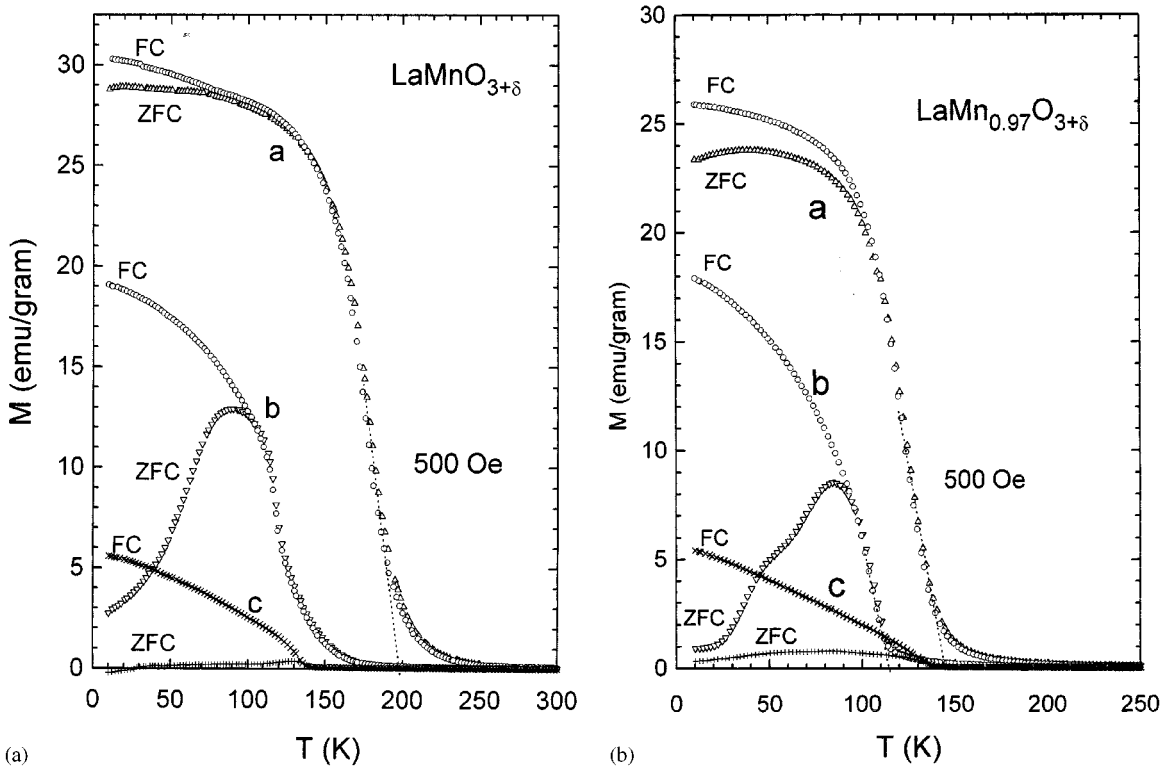

FIG. 11. Temperature dependence of magnetization for $LaMnO_{3+\delta}$ (a): Oxygen reduction treatments given are a, as-prepared, b, 118 Pa desorption, and c, vacuum-treated. For $La_{0.97}MnO_{3+\delta}$ (b): they are a, as-prepared, b, 185 Pa desorption, and c, vacuum-treated. Corresponding lattice parameters and estimated δ values are listed in Table 1.

preferentially at the La site (3, 9). Since the La/Mn ratio is kept constant on incorporation of excess oxygen, the La site vacancy model inevitably requires precipitation of La_2O_3 or occupation of the La ions on the Mn site according to

$$LaMnO_{3+\delta} + \frac{\delta}{2} O_2 = \frac{3+\delta}{3} \{La^{3+}_{1-2\delta/(3+\delta)} V_{2\delta/(3+\delta)}\}$$

$$\times \{Mn^{3+}_{3(1-2\delta)/(3+\delta)}\ Mn^{4+}_{3\cdot 2\delta/(3+\delta)} La^{3+}_{\delta/(3+\delta)}\}\ O_3^{2+}. \qquad [21]$$

To explain the upper limit of δ, Mizusaki *et al.* (9) introduced a site exclusion model assuming a spherical vacancy exclusion space consisting of nine unit cells (nine La ions) and only a single La ion inside this sphere can enter into a Mn site to create a La site vacancy. Consequently, the La concentration available for the vacancy formation decreases and is given by $1 - 9\{2\delta/(3+\delta)\} = (3 - 17\delta)/(3+\delta)$, instead of $1 - 2\delta/(3+\delta)$ given by Eq. [21], yielding the upper limit of δ, $\delta_{max} = 3/17 = 0.1764$.

Here, we formulate the La site vacancy model by considering the entropy of mixing for the La site vacancies and compare it with the present La and Mn site vacancy model (Eq. [3]). Our interest lies in how the different defect site models affect the calculated isotherms. The defect equilibrium can be expressed by

$$6Mn^{3+} + La^{3+}(La) + \tfrac{3}{2} O_2 = 6Mn^{4+} + 3O^{2-}$$

$$+ La^{3+}(Mn) + 2V_{La}. \qquad [22]$$

Here, $La^{3+}(La)$ and $La^{3+}(Mn)$ mean La^{3+} in the La and in the Mn sites, respectively. For the equilibrium Eq. [21] gives $[V_{La}] = 2\delta/(3+\delta)$, $[La^{3+}(Mn)] = \delta/(3+\delta)$, $[Mn^{3+}] = 3(1-2\delta)/(3+\delta)$, $[Mn^{4+}] = 3\cdot 2\delta/(3+\delta)$, and $[Mn^{3+}] + [Mn^{4+}] = 3/(3+\delta)$. Considering the number of La atoms within a vacancy exclusion space, η_L, and assuming the random mixing of Mn^{4+} and Mn^{3+} ions, we obtain the following equation for the chemical potential for the three oxygen ions:

$$3\mu_O = 3\mu_O^\circ(T) + RT \ln \left\{\frac{\eta_L 2\delta/(3+\delta)}{1 - \eta_L 2\delta/(3+\delta)}\right\}^2$$

$$+ RT \ln \left(\frac{2\delta}{1-2\delta}\right)^6 + RT \ln \left\{\frac{\delta/(3+\delta)}{1-\delta/(3+\delta)}\right\}$$

$$= 3\mu_O^\circ(T) + RT \ln f_L(\delta). \qquad [23]$$

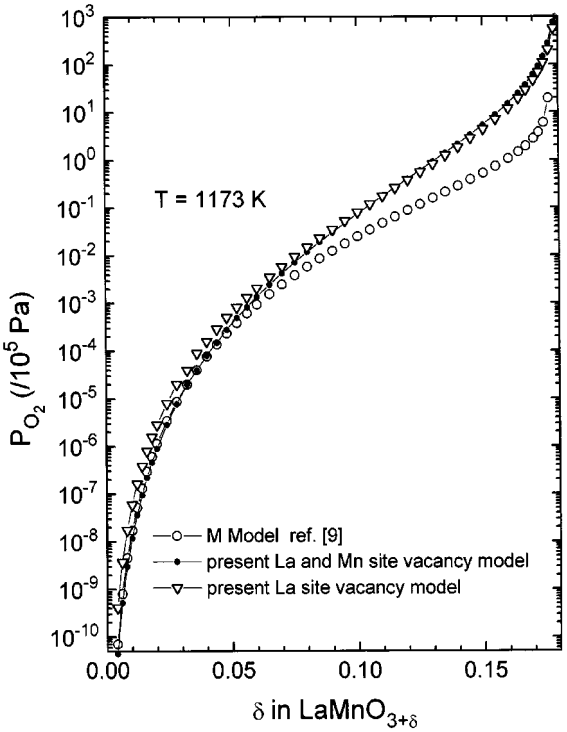

FIG. 12. P–δ–T isotherms at 1173 K calculated on the basis of the three different models.

The last expression of Eq. [23] is the definition of $f_L(\delta)$. To compare Eq. [23] with Eq. [3], we substitute $\eta_L = \eta/2 = 8.83$ into Eq. [23] ($\eta = 17.67$ in Eq. [3], $\delta_{max} = 0.18$), instead of Mizusaki's value 9.0. Using Eq. [6], the equilibrium constant K_L is given by

$$K_L = \exp\left\{\frac{-\Delta\mu^\circ(T)}{RT}\right\} = f_L(\delta)P_{O_2}^{-3/2}. \qquad [24]$$

Figure 12 compares the P–δ–T isotherms at $T = 1173$ K calculated from the three different models, that is, the present vacancy exclusion model (Eqs. [3]–[7]) and the two models of vacancies occupying exclusively the La site (Eqs. [15] and [16] and [23] and [24]). The difference between the latter two models arises simply from the different formulations, that is, the law of mass action and the entropy of mixing as discussed in Section 2. Figure 12 tells us that the difference between the two models, Eqs. [3]–[7] and [23] and [24] is very small indeed. Examination of Eqs. [3] and [23] shows that the entropy of mixing terms for vacancies and Mn^{4+} are identical. This is because both models predict the same number of vacancies, whether the vacancies are located only on the La site or on both the La and Mn sites. This means that the difference in $\eta = 17.67$ ($\eta\delta/(3+\delta)$ in Eq. [3]) and $\eta_L = 8.83$ ($\eta_L 2\delta/(3+\delta)$ in Eq. [23]) is compensated by a factor of 2 in the vacancy concentration in Eq. [23]. The only difference, therefore, is due to the difference in the entropy of mixing arising from La in the Mn site, which turns out to have little affect on the calculated isotherms. Therefore, it is almost impossible to tell from the P–δ–T relation which model is better to describe the actual vacancy distribution in $LaMnO_{3+\delta}$.

It is known that the substitution of cations (vacancies) for the Mn site results in a significant decrease in the magnetic ordering temperature (18–21). Moreover, the substitution of cations, such as $Mg^{2+}$and Fe^{3+}, causes ferromagnetic to spin glass transition. If La ions enter into the Mn sites, the amount of La^{3+} in the Mn site is given by $\delta/(3+\delta)$ from Eq. [21], i.e., $0.15/3.15 = 0.0476$ for $LaMnO_{3.15}$. If such a significant amount of La^{3+} ions, 4.76%, enter into the Mn site, the ferromagnetic transition temperature should decrease appreciably and ZFC magnetization vs temperature curve must show the spin glass-like behavior. The T_c vs δ relation for $LaMnO_{3+\delta}$ (5, 6) and the FC and ZFC magnetization curves shown in Figs. 11a and 11b are not consistent with the above argument because with increasing δ, T_c increases and the difference between ZFC and FC almost vanishes.

5.2. *Origin of Hysteresis in P–δ–T Isotherms*

The most conspicuous feature of the observed P–δ–T relation is the existence of hysteresis. The equilibrium pressure at a given δ is always lower in the desorption process than in the absorption process. The hysteresis becomes enhanced when the sample is degassed under dynamic vacuum for a long period of time until the excess oxygen becomes almost zero as shown in Fig. 9. Such a type of hysteresis is well known in the metal–hydrogen system and usually appears when the hydride is formed during the absorption and is decomposed during the desorption process, respectively (22). In the $La_{0.9}MnO_{3+\delta}$ system, significant hysteretic effects in the magnetization and resistivity properties were reported when the sample was subjected to the deoxidization and oxidation cycle in Ar and oxygen atmospheres at 1373 K (23). The sample deoxidized in the Ar atmosphere was reported never to recover its initial magnetization and resistivity values even after the oxidation treatment was made on the sample.

At the moment, we do not know the origin of this type of hysteresis (Fig. 9). When oxygen atoms enter into interstitial or oxygen vacant sites such as vacant chain positions in $YBa_2Cu_3O_{7-\delta}$, no significant hysteresis was reported so far. Thus, it is likely that the formation and annihilation of cation vacancies accompanied by the oxygen absorption and desorption are the cause of the observed hysteresis. It is noted that we must specify the desorption or absorption process employed whenever the P–δ–T relationship is measured for $LaMnO_{3+\delta}$.

6. SUMMARY

To understand the P–δ–T isotherms of $LaMnO_{3+\delta}$, we have proposed a defect model in which the first 6 and second 12 nearest neighboring La (Mn) sites around a La (Mn) site vacancy are excluded from the additional formation of vacancies. The P–δ–T relation calculated on the basis of the above model is found to explain the P–δ–T relation observed at 1073 to 1273 K. The volumetric method has been used to measure the P–δ–T relationship during the desorption process. A significant hysteresis is noted in the P–δ–T isotherms during the desorption and absorption processes. The hysteresis is found to be enhanced in the absorption process after the δ value of the $LaMnO_{3+\delta}$ sample is desorbed closer to zero. We have calculated the P–δ–T isotherms for the two models, namely, (1) the excess oxygen atoms create equal amounts of La and Mn site vacancies and (2) they create only La site vacancies with the excess La ions located in the Mn site. No significant difference is observed between the P–δ–T isotherms calculated for the two models. The ZFC and FC magnetization vs temperature relations, however, suggest that the La and Mn vacancy model is preferable to the La site vacancy model.

REFERENCES

1. G. H. Jonker and J. H. Van Saten, *Physica* **16,** 337 (1950); **19,** 120 (1953).
2. E. O. Wollen and W. C. Koehler, *Phys. Rev.* **100,** 545 (1955).
3. B. C. Tofield and W. R. Scott, *J. Solid State Chem.* **10,** 183 (1974).
4. I. G. Krough Andersen, E. Krough Andersen, P. Norby, and E. Skou, *J. Solid State Chem.* **113,** 320 (1994).
5. J. Toepfer and J. B. Goodenough, *J. Solid State Chem.* **130,** 117 (1997).
6. J. Toepfer and J. B. Goodenough, *Chem. Mater.* **9,** 1467 (1977).
7. J. A. M. Roosmalen and E. H. P. Cordfunke, *J. Solid State Chem.* **110,** 106 (1994); **109** (1994); **113** (1994).
8. J. H. Kuo and H. U. Andersen, *J. Solid State Chem.* **83,** 52 (1989).
9. J. Mizusaki, N. Mori, H. Takai, Y. Yonemura, H. Minamiue, H. Tagawa, M. Doiya, H. Inaba, K. Naraya, T. Sasamoto, and T. Hashimoto, *Solid State Ionics* **129,** 163 (2000).
10. J. Nowotny and M. Rekas, *J. Am. Ceram. Soc.* **81,** 67 (1998).
11. K. Nakamura, M. Xu, M. Klaeser, and G. Linker, *J. Solid State Chem.* **156,** 143 (2001).
12. Y. Takeda, S. Nakai, T. Kojima, R. Kanno, N. Imanishi, G. Q. Shen, O. Yamamoto, M. Mori, C. Asakawa, and T. Abe, *Mater. Res. Bull.* **26,** 153 (1991).
13. K. Nakamura, J. Ye, and A. Ishii, *Physica C* **213,** 1 (1993).
14. P. A. Redhead, J. P. Hobson, and E. V. Koornelsen, "The Physical Basis of Ultrahigh Vacuum". Chapman and Hall, London, 1968.
15. J. F. Mitchell, D. N. Argyriou, C. D. Potter, D. G. Hinks, J. D. Jorgensen, and S. D. Buder, *Phys. Rev. B* **54,** 6172 (1966).
16. G. H. Jonker, *Physica* **22,** 707 (1956).
17. J. A. M. Roosmalen, D. van Vlaaderen, E. H. P. Cordfunke, W. L. Ljdo, and D. J. W. Ijdo, *J. Solid State Chem.* **114,** 516 (1995).
18. A. Anane, C. Dupas, K. Le Dang, J. P. Renard, P. Veillet, L. Pinsard, and A. Revcolevschi, *Appl. Phys. Lett.* **69,** 1160 (1996).
19. K. H. Ahn, X. W. Wu, K. Liu, and C. L. Chien, *Phys. Rev. B* **54,** 15299 (1996).
20. J. W. Cai, C. Wang, B. G. Shen, J. G. Ahao, and W. S. Zhan, *Appl. Phys. Lett.* **71,** 1727 (1997).
21. K. Nakamura, X. Liu, T. Hatano, Z. Jiao, K. Shang, and A. Ishii, *Jpn. J. Appl. Phys.* **39,** 1721 (2000).
22. J. J. Reilly and R. H. Wiswall, Jr., *J. Inorg. Chem.* **13,** 219 (1974).
23. T. R. Mcguire, P. R. Duncombe, G. Q. Gong, A. Gupta, X. W. Li, S. J. Pickart, and M. L. Crow, *J. Appl. Phys.* **83,** 7076 (1998).